PROCEEDINGS, Fire and Evacuation Modeling Technical Conference (FEMTC) 2024
Kansas City, Missouri, September 18-20, 2024

Recent Developments in the Fire Dynamics Simulator (FDS)

Kevin McGrattan
National Institute of Standards and Technology
Gaithersburg, Maryland, USA
email: kevin.mcgrattan@nist.gov

Jonathan L. Hodges
Jensen Hughes
Blacksburg, Virginia, USA
email: jhodges@jensenhughes.com

Jason Floyd
Fire Safety Research Institute, UL Research Institutes
Columbia, Maryland, USA
email: jason.floyd@ul.org

ABSTRACT

This paper describes two new features in the Fire Dynamics Simulator: (1) a simplified burning model that makes use of bench-scale burning rate measurements scaled by the incoming heat flux, and (2) three-dimensional heat conduction.

S-PYRO, SCALING PYROLYSIS

A key decision made by fire modelers is whether to *specify* or *predict* the burning rate of real materials. For those choosing to specify, even if full-scale burning rate data is available, there is still an issue as to whether an item burned under a calorimeter will burn at the same rate as an item in an enclosure. For those choosing to predict, the number of parameters required by even simple kinetics models can make the problem intractable. An approach that falls somewhere in between specifying and predicting the heat release rate is to apply the measured burning rate from a device like the cone calorimeter at the surface of a solid object once the surface temperature has reached some specified "ignition temperature." This technique has been the mainstay of FDS modeling over the past 20 years.

Recently, an enhancement of this approach has been developed that addresses its fundamental weakness; that is, the burning rate obtained from the cone calorimeter is dependent on the exposing heat flux and sample thickness. The solution is to scale the measured burning rate to account for varying heat flux and solid thickness in the simulation. The shape of the heat release rate with time is preserved, but its magnitude and duration scale with the incident heat flux and thickness. The model is able to scale a single reference curve to different thermal exposures and material thicknesses. An empirical estimation of the flame heat flux is used to calculate the total incident heat flux in a cone calorimeter for use in scaling. Improved agreement can be achieved by incorporating data from multiple cone calorimeter experiments at different thermal exposures

and/or material thicknesses. The following subsections describe the technical basis of each of these modules.

Fixed Thickness Scaling Model

The fixed thickness scaling based pyrolysis model is presented in [2]. The net heat flux into the material is related to the pyrolysis rate through the effective heat of gasification according to the equation

$$\dot{q}''_{\text{net}} = \dot{m}''_{\text{f}} \Delta h_{\text{g}} \tag{1}$$

where $\dot{q}''_{\text{net}}$ is the net heat flux into the surface and Δh_{g} is the heat of gasification. Similarly, the heat release rate per unit area of a material, $\dot{Q}''$, is related to the pyrolysis rate of the material through the effective heat of combustion, Δh, as

$$\dot{Q}'' = \dot{m}''_{\text{f}} \Delta h \tag{2}$$

The ratio of Eq. (1) and Eq. (2) relate $\dot{q}''_{\text{net}}$ and $\dot{Q}''$ as

$$\frac{\dot{Q}''}{\dot{q}''_{\text{net}}} = \frac{\Delta h}{\Delta h_{\text{g}}} \tag{3}$$

Assuming Δh_{g} and Δh are invariant with $\dot{q}''_{\text{net}}$, Eq. (3) can be related to predict the change in magnitude of $\dot{Q}''$ due to changes in thermal exposure as

$$\dot{Q}''_1 = \frac{\dot{q}''_{\text{net},1}}{\dot{q}''_{\text{net},2}} \dot{Q}''_2 \tag{4}$$

where the subscripts 1 and 2 indicate different thermal exposure levels. The acceleration or deceleration of the burning can be calculated by evaluating the difference in time required to release the same amount of energy at the two $\dot{Q}$ over a discrete time interval, Δt,

$$E''_{\Delta t} = \dot{q}''_{\text{net}} \frac{\Delta h}{\Delta h_{\text{g}}} \Delta t \tag{5}$$

where $E_{\Delta t}$ is the total energy released over Δt. Relating Eq. (5) at two thermal exposure levels yields

$$\Delta t_1 = \frac{\dot{q}''_{\text{net},2}}{\dot{q}''_{\text{net},1}} \Delta t_2 \tag{6}$$

Because $\dot{q}''_{\text{net}}$ is difficult to measure during burning, an approximate reference heat flux, $\dot{q}''_{\text{ref}}$, is introduced as

$$\dot{q}''_{\text{ref}} = \dot{q}''_{\text{cone}}(1 - \Gamma) + \dot{q}''_{\text{flame}} \tag{7}$$

where $\dot{q}''_{\text{cone}}$ is the set exposure flux to a cold surface in the cone calorimeter testing, Γ is the fraction of that flux absorbed by the flame, and $\dot{q}''_{\text{flame}}$ is the heat feedback from the flame to the surface. For the input data from a cone test, the values of Γ and $\dot{q}''_{\text{ref}}$ are not readily obtained, and the empirical approach discussed in the *Cone Reference Heat Flux* section is used to estimate them when determining $\dot{q}''_{\text{net},2}$ in Eq. 4. For $\dot{q}''_{\text{net},1}$, FDS uses the sum of the incident radiation and the net convective heat flux in the calculation at each time step.

Adaptation to Multiple Thicknesses

Detailed pyrolysis models are typically based on an Arrhenius kinetics formulation [3]:

$$r = A\mathrm{e}^{-E/(RT_\mathrm{s})}\zeta_1\zeta_2...\zeta_\mathrm{N} \tag{8}$$

where r is the reaction rate, A and E are the Arrhenius pre-exponential factor and activation energy, T_s is the solid temperature, R is the molar gas constant, and ζ_j is the impact of the j-th reactant species concentration on the burning. There are two primary impacts of material thickness on the burning behavior of a material. The largest impact is to the burning duration due to differences in the combustible mass. The second impact is the transition between a thermally thin and thermally thick material. The model for scaling to different material thicknesses takes inspiration from this formulation; however, the model assumes that the two impacts can be represented by a non-dimensional scaling of a measured burning profile.

The non-dimensional temperature profile within a solid material scales with the Fourier, Fo, and Biot, Bi, numbers. Fo is the ratio of the heat conduction rate to the rate of thermal energy storage in a solid, and can be thought of as a dimensionless time [1]. It is defined as

$$\mathrm{Fo} = \frac{\alpha}{\Delta^2}t = \frac{k}{\rho c_p \Delta^2}t \tag{9}$$

where α is the thermal diffusivity, ρ is the density, c_p is the specific heat capacity, k is the thermal conductivity, Δ is the thickness, and t is time. Bi is the ratio of the internal thermal resistance of a solid to the external resistance of the surface boundary layer [1]:

$$\mathrm{Bi} = \frac{h}{k/\Delta} \tag{10}$$

where h is the heat transfer coefficient (where h is traditionally the convective heat transfer coefficient, h_c, but can also be a combination of h_c and an effective radiation heat transfer coefficient [1]). The traditional formulation of Bi assumes that the external exposure of the solid is related primarily to surface convection and thus uses the convection heat transfer coefficient, h_c, for h. However, this assumption is not valid in the case of burning solid fuels where external radiation (such as the applied surface heat flux in a cone calorimeter experiment) and flame radiation from the combustion of pyrolyzate above the surface drive the heat transfer to the surface. This is accounted for with an alternative Biot number, Bi*, which combines the effect of surface convection and radiation:

$$\mathrm{Bi}^* = \frac{h_\mathrm{c} + h_\mathrm{r}}{k/\Delta} \tag{11}$$

where h has been split into two components for convection, h_c, and radiation, h_r. The radiation heat transfer coefficient is calculated based on the linearized formulation [1]:

$$h_\mathrm{r} = \varepsilon\sigma\left(T_\mathrm{r} + T_\mathrm{s}\right)\left(T_\mathrm{r}^2 + T_\mathrm{s}^2\right) \tag{12}$$

where ε is the surface emissivity, σ is the Stefan-Boltzmann constant, T_r is the radiative temperature, and T_s is the surface temperature. The radiative temperature is an effective temperature representative of the energy absorbed at the surface assuming a view factor of 1:

$$T_\mathrm{r} = \left[\frac{\dot{q}''_\mathrm{r}}{\varepsilon\sigma}\right]^{\frac{1}{4}} \tag{13}$$

where $\dot{q}''_{\mathrm{r}}$ is the incident radiation to the surface.

As discussed above, Δh_{g} is assumed to be constant in the prior approach. However, a time-varying effective Δh_{g} can be calculated based on Eq. (3) using the time-varying measurement of $\dot{Q}''$ and estimating the time-varying $\dot{q}''_{\mathrm{flame}}$. It is assumed in this model that the variability in burning intensity and duration observed in experiments can be related to the impact of the material thickness and thermal exposure on these non-dimensional groups, $\Delta h_{\mathrm{g}} = f\left(\mathrm{Bi}^*, \mathrm{Fo}\right)$. Δh_{g} was found to collapse at the non-dimensional time-scale FoBi^*. A scaling relationship for FoBi^* can be established by equating this non-dimensional time across two exposure levels,

$$\mathrm{FoBi}^* = \frac{h_1 t_1}{\rho_1 c_{p,1} \Delta_1} = \frac{h_2 t_2}{\rho_2 c_{p,2} \Delta_2} \tag{14}$$

where the subscripts indicate different exposure levels. Equation (14) reveals that non-dimensional time scales with ρ, c_p, Δ, and h.

A simplified representation for the scaling of non-dimensional time can be obtained by assuming that changes in material properties (i.e., k, ρ, c_p) are related to non-dimensional time. Under this assumption, Eq. (14) reduces to:

$$t_2 = \frac{\Delta_2}{\Delta_1} \frac{h_1}{h_2} t_1 \tag{15}$$

In the case of constant thickness (i.e., $\Delta_1 = \Delta_2$), Eq. (15) is consistent with Eq. (6) across a discrete time interval. Thus, the ratio of h scales similarly to the ratio of $\dot{q}''$, yielding:

$$\Delta t = \frac{\Delta}{\Delta_{\mathrm{ref}}} \frac{\dot{q}''_{\mathrm{ref}}}{\dot{q}''} \Delta t_{\mathrm{ref}} \tag{16}$$

Cone Reference Heat Flux

When using Eq. 7 to obtain $\dot{q}''_{\mathrm{net},2}$ in Eq. 4, an approach is needed to determine Γ and $\dot{q}''_{\mathrm{flame}}$. In an actual cone test these will depend upon the material being burned as the heat of combustion, burning rate, and soot yield will all influence the flame heat flux and the absorption of the cone radiation. As there is no simple analytical model to predict these, an empirical approach was developed using FDS simulations of a cone calorimeter.

The simulation geometry is shown in Fig. 1 and includes the radiant cone, the sample holder, and a volume above the cone to capture the flame height contribution to the heat feedback. A set of 30 simulations were run where the heat of combustion (10, 20, 30, 40, and 50 MJ/kg) and soot yield (0, 1, 2, 5, 10, and 20 %) were varied (CO yield was assumed to equal the soot yield). Each simulation consisted of three phases: the sample burning at a prescribed rate with the cone off, the sample burning at a prescribed rate with the cone on, and no burning with the cone on ($\dot{q}''_{\mathrm{cone}} = 50$ kW/m^2). The prescribed burning was varied over a range of HRRPUA (100, 200, 400, 800, 1200, 1600, and 2000 kW/m^2). The sample was given a fixed temperature of 300 °C representing a notional ignition temperature. The cone off phase gives $\dot{q}''_{\mathrm{flame}}$, the delta between burning with the cone on and burning with the cone off and on gives the cone flux reaching the sample, and the cone with no burning phase gives $\dot{q}''_{\mathrm{cone}}$. The difference between the cone flux reaching the sample and $\dot{q}''_{\mathrm{cone}}$ gives Γ.

A notional fuel molecule was created for each heat of combustion and soot yield that provided an oxygen heat of combustion (EPUMO2) of 13,100 kJ/kg. For a 0 % soot yield, the following was

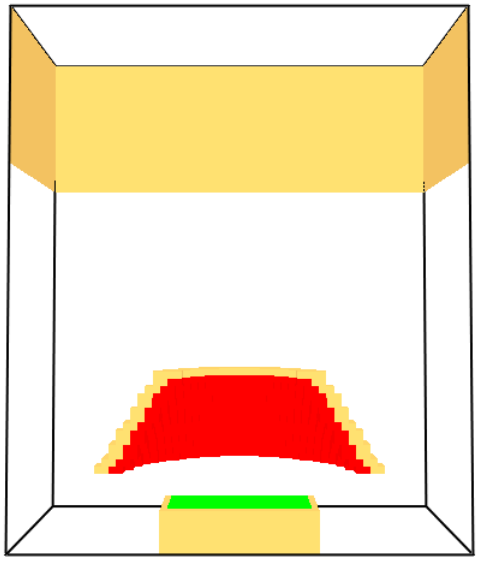

Figure 1: FDS geometry used for developing the cone reference flux. Red is the cone heater and green is the sample surface. The domain is clipped at the plane y=0 m.

done to obtain fuel chemistry. A heat of combustion of 50 MJ/kg implies a fuel like methane and the formula $CH_{3.333}$ provides the desired EPUMO2 at a soot yield of 0 %. A heat of combustion of 40 MJ/kg implies a hydrocarbon like fuel, and the resulting formula is $CH_{0.959}$. For 10, 20 and 30 MJ/kg oxygen was added while keeping a C:H ratio of 1:2, resulting in formulas of $CH_2O_{0.302}$, $CH_2O_{0.658}$, and $CH_2O_{1.322}$. The H or O values were varied as needed for the different soot yields to keep an EPUMO2 of 13,100 kJ/kg.

If $\dot{q}''_{\text{flame}}$ for each heat of combustion is normalized by the maximum value for all HRRPUA, the results collapse as shown in the left of Fig 2. We can then determine a quadratic fit for the maximum $\dot{q}''_{\text{flame}}$ as a function of heat of combustion as shown in the right of Fig 2.

Various simple combinations of the heat of combustion, soot yield, and HRRPUA were evaluated to determine a relationship for Γ. The functional form of $A + B \times \text{HRRPUA}/\Delta h + C \times \text{soot yield}$ gave a fit with the lowest RMS value. To determine the time-dependent $\dot{q}''_{\text{ref}}$ for a cone test, first, the maximum $\dot{q}''_{\text{flame}}$ is determined using Δh at the fit shown in Fig 2, second, $\dot{q}''_{\text{flame}}$ is adjusted for the current HRRPUA by interpolating the average normalized curve in Fig 2, third, Γ is determined and used to adjust $\dot{q}''_{\text{cone}}$, and finally, $\dot{q}''_{\text{ref}}$ is determined via Eq. 7. The resulting fit has a 2 % error compared to the FDS predictions, see Fig. 3.

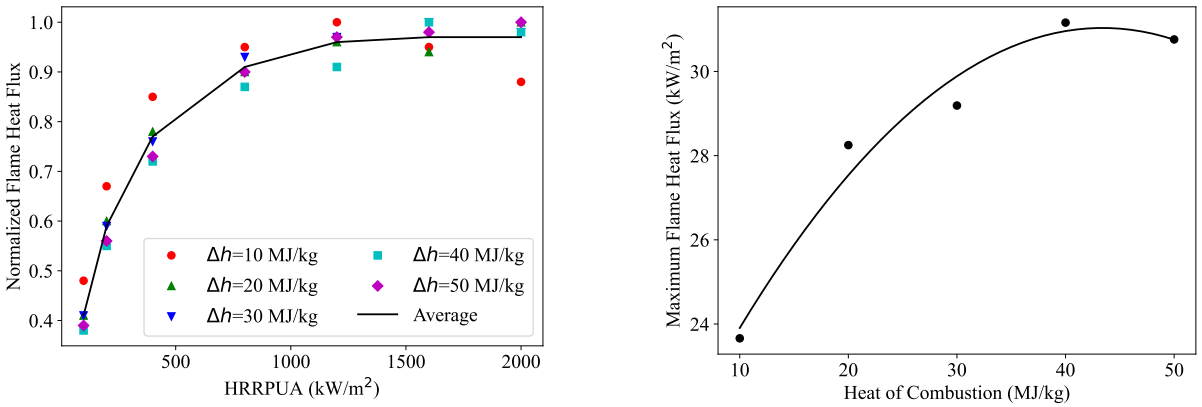

Figure 2: (Left) Normalized flame heat flux as a function of HRRPUA. (Right) Maximum flame heat flux as a function of Δh.

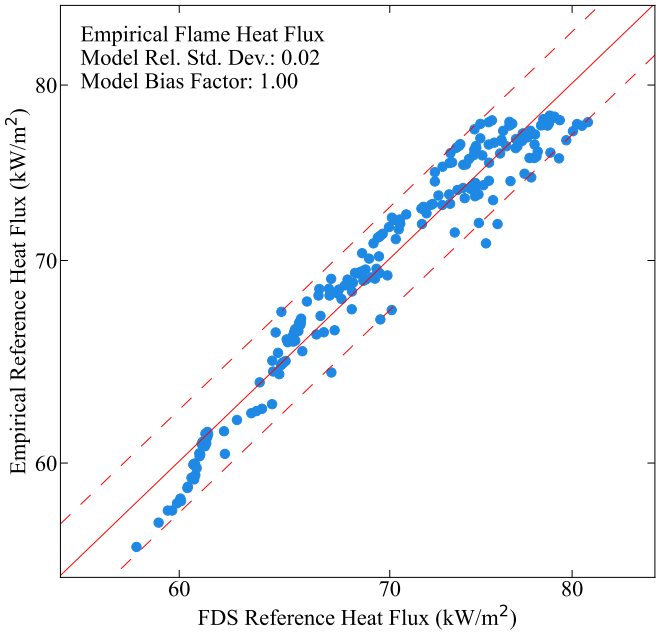

Figure 3: Scatterplot for predicted vs. empirical reference heat flux.

THREE-DIMENSIONAL HEAT CONDUCTION IN SOLIDS

For most FDS simulations, a very good assumption is that heat conduction in solids is primarily in the direction normal to the surface. After all, most of the obstructions in a building environment are insulated walls, ceilings, floors, and furnishings. However, there are scenarios for which the lateral conduction of heat along a solid surface might be important, as in the case of structural steel. For these, three-dimensional heat conduction is warranted, but within a model like FDS, it is difficult and computationally expensive to apply. Moreover, there are several finite element-based thermal/structural models that specialize in the complicated geometry of beams, columns and other structural members.

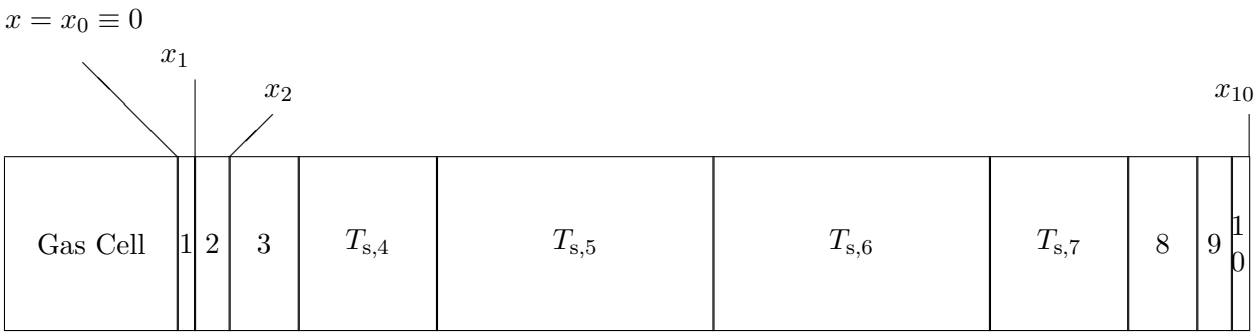

Figure 4: Layout of solid phase cells. In this example, each solid phase cell is stretched by a factor of 2 until the halfway point of the solid is reached, after which the cells shrink by a factor of 2. The interface between gas and solid phase is at x_0. The back side boundary condition is applied at x_{10}.

As with the S-Pyro model described above, there is an intermediate approach between simple 1-D heat conduction performed by FDS and full 3-D heat conduction performed by another model. This approach exploits the existing 1-D heat conduction solver, but extends it in limited circumstances to 3-D. The 1-D heat conduction equation in Cartesian coordinates is:

$$\rho_s c_s \frac{\partial T_s}{\partial t} = \frac{\partial}{\partial x}\left(k_s \frac{\partial T_s}{\partial x}\right) + \dot{q}_s''' \tag{17}$$

The indexing system used for the discretization of the equations is shown in Fig. 4. The discretization scheme is the same regardless of whether the coordinate system is Cartesian, cylindrical, or spherical. The size of the cell nearest the boundary is set by default to be

$$x_1 - x_0 = \sqrt{\frac{\delta t_0 \; k_s}{\rho_s \, c_s}} \tag{18}$$

where δt_0 is a somewhat arbitrary time scale set to 1. In other words, the Fourier number based on the cell size is assumed of order unity. The user has flexibility in changing both the initial cell size and the degree of stretching.

The temperature at the center of each solid cell, $T_{s,i}$, is updated in time using a Crank-Nicolson scheme:

$$\begin{aligned}(\rho_s \, c_s)_i \frac{T_{s,i}^{n+1} - T_{s,i}^{n}}{\delta t} = {} & \frac{1}{2 \; \delta x_i}\left(k_{s,i+\frac{1}{2}} \frac{T_{s,i+1}^{n} - T_{s,i}^{n}}{\delta x_{i+\frac{1}{2}}} - k_{s,i-\frac{1}{2}} \frac{T_{s,i}^{n} - T_{s,i-1}^{n}}{\delta x_{i-\frac{1}{2}}}\right) \\ & + \frac{1}{2 \, \delta x_i}\left(k_{s,i+\frac{1}{2}} \frac{T_{s,i+1}^{n+1} - T_{s,i}^{n+1}}{\delta x_{i+\frac{1}{2}}} - k_{s,i-\frac{1}{2}} \frac{T_{s,i}^{n+1} - T_{s,i-1}^{n+1}}{\delta x_{i-\frac{1}{2}}}\right) + \dot{q}_{s,i}'''\end{aligned} \tag{19}$$

$k_{s,i+\frac{1}{2}}$ is the thermal conductivity at the border of the cells i and $i+1$, δx_i is the width of cell i, and $\delta x_{i+\frac{1}{2}}$ is the distance from the center of cell i to the center of cell $i+1$.

The solid phase heat conduction equation in three directions is given by:

$$\rho_s c_s \frac{\partial T_s}{\partial t} = \frac{\partial}{\partial x}\left(k_s \frac{\partial T_s}{\partial x}\right) + \frac{\partial}{\partial y}\left(k_s \frac{\partial T_s}{\partial y}\right) + \frac{\partial}{\partial z}\left(k_s \frac{\partial T_s}{\partial z}\right) + \dot{q}_s''' \tag{20}$$

The method of solution is to split this equation using the following alternating direction implicit (ADI) scheme:

$$\frac{\rho_s c_s}{3}\frac{\partial T_s}{\partial t} = \frac{\partial}{\partial x}\left(k_s \frac{\partial T_s}{\partial x}\right) + \frac{\dot{q}_s'''}{3} \tag{21}$$

$$\frac{\rho_s c_s}{3}\frac{\partial T_s}{\partial t} = \frac{\partial}{\partial y}\left(k_s \frac{\partial T_s}{\partial y}\right) + \frac{\dot{q}_s'''}{3} \tag{22}$$

$$\frac{\rho_s c_s}{3}\frac{\partial T_s}{\partial t} = \frac{\partial}{\partial z}\left(k_s \frac{\partial T_s}{\partial z}\right) + \frac{\dot{q}_s'''}{3} \tag{23}$$

The solution of the equation is updated over the course of three gas phase time steps of size δt. For each coordinate direction, the temperature field is finely gridded near the surface and coarsely gridded in the interior, typically. Thus, the temperature field, $T_s(x, y, z, t)$, is discretized differently in each direction. For example, for each surface cell normal to the x direction, the 1-D temperature array in depth is $T_{s,x,i}$, where $1 \le i \le N_x$, and N_x is the number of non-uniformly spaced internal cells spanning the entire width of the solid in the x direction. This is exactly the same approach taken above for 1-D heat conduction in solids with "exposed" back surfaces. Likewise, $T_s(x, y, z, t)$ is discretized $T_{s,y,j}$ and $T_{s,z,k}$ in the y and z directions, respectively.

In each of the three steps, the 1-D heat conduction equation is solved in one of the three coordinate directions using the Crank-Nicolson (C-N) scheme described above, except now the implicit update spans three gas phase time steps, $3\,\delta t$. The temperature fields spanning the other two coordinate directions are updated explicitly. The change in temperature due to the implicit C-N update is denoted $\Delta T_{s,x,i}$, with similar expressions for the y and z updates. The explicit update taken during the two steps for which $T_{s,x,i}$ is not updated implicitly transfers enthalpy in the y and z directions:

$$\rho_{s,i} c_{s,i} T_{s,x,i}^{n+1} = \rho_{s,i} c_{s,i} T_{s,x,i}^{n} + \frac{1}{2}\left[\sum_j w_j \rho_{s,j} c_{s,j} \Delta T_{s,y,j} + \sum_k w_k \rho_{s,k} c_{s,k} \Delta T_{s,z,k}\right] \tag{24}$$

The coefficients, w_j and w_k, are the fractions of cell i of the x direction discretization overlapped by cells j and k of the y and z discretizations, respectively.

This type of splitting scheme is discussed by Toro [4], Chapter 16, "Methods for Multi-Dimensional PDEs."

The purpose of this test case is to compare FDS HT3D with a well-established commercial finite-element model (ANSYS) for a reasonably practical problem. We consider a steel I-beam cross-section 0.4 m on each side. The flanges are 6 cm thick and the web is 4 cm thick. The grid resolution for both FEM and FDS models is $\Delta x = 1$ cm. The thermal properties of the steel are taken to be constant: $k = 45$ W/(m K), $\rho = 7850$ kg/m^3, and $c = 0.60$ kJ/(kg K). The boundary conditions are adiabatic except for a hot patch on the front half of the bottom flange maintained at 800 °C. The initial temperature of the steel is 20 °C and the case is run for 3600 s. Note that the FEM model is run with a time step comparable to the explicit stability criterion ($\Delta t \approx 1.7$ s) in order to yield time accurate results for comparison with FDS.

Figure 5 shows a comparison between the surface temperature contours from ANSYS (left) and FDS (right). Below that, in Fig. 6, we show the time history of the surface temperatures for six locations on the bottom flange (positions may be identified from the image on the left).

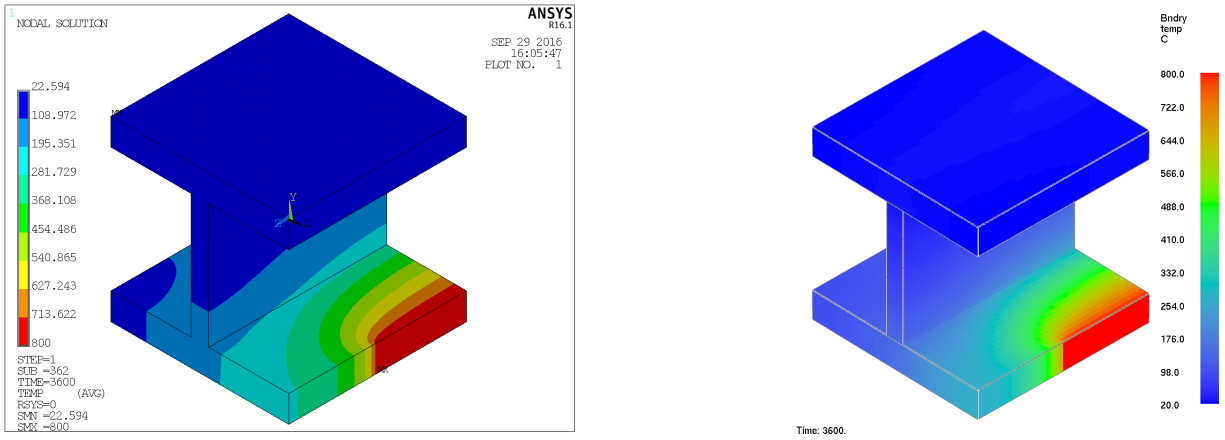

Figure 5: Three-dimensional heat diffusion in an I-beam, comparison between a commercial finite-element code (ANSYS, left, courtesy Chao Zhang) and FDS (right). The beam boundary conditions are adiabatic except for a hot patch maintained at 800 °C *on the front right of the bottom flange. The initial temperature of the steel is* 20 °C *and the calculations are run for* 3600 s.

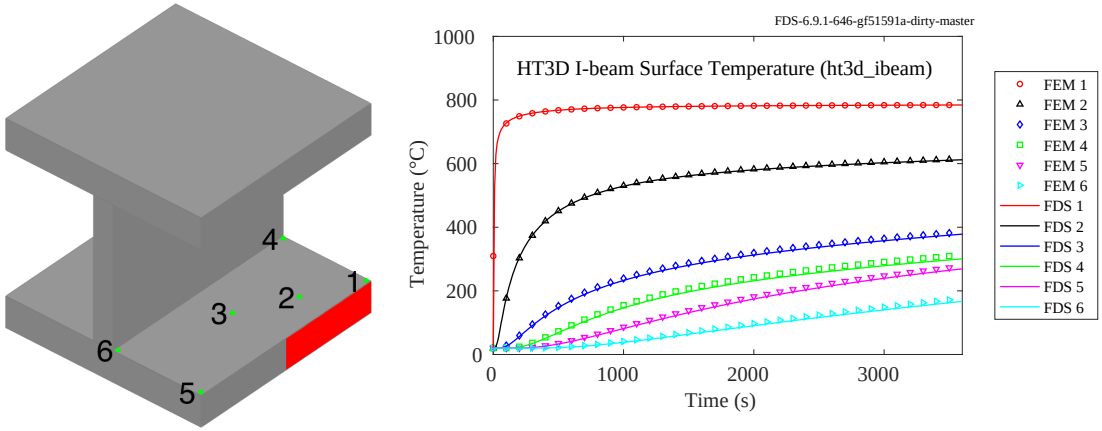

Figure 6: (Left) Device locations corresponding to the legend entries in the plot to the right. (Right) Time history of the surface temperature. Symbols represent the finite-element model (FEM) results and the lines represent the FDS results.

REFERENCES

[1] T.L. Bergman et al. *Fundamentals of Heat and Mass Transfer*. 7th. New York: John Wiley and Sons, 2011.

[2] Jonathan L Hodges et al. "An Engineering Model for the Pyrolysis of Materials". In: *Fire Safety Journal* 141.September (2023), p. 103980. ISSN: 0379-7112. DOI: 10.1016/j.firesaf.2023.103980.

[3] Stanislav I. Stoliarov and Yan Ding. "Pyrolysis Model Parameterization and Fire Growth Prediction: The State of the Art". In: *Fire Safety Journal* 140 (2023), p. 103905. ISSN: 03797112. DOI: 10.1016/j.firesaf.2023.103905.

[4] E.F. Toro. *Riemann Solvers and Numerical Methods for Fluid Dynamics: A Practical Introduction*. 2nd. Springer, 1999.